OCEANOGRAPHY

Algal plankton turn to hunting to survive and recover from end-Cretaceous impact darkness

Samantha J. Gibbs[1]*†, Paul R. Bown[2†], Ben A. Ward[1†], Sarah A. Alvarez[3,2], Hojung Kim[2], Odysseas A. Archontikis[2‡], Boris Sauterey[4], Alex J. Poulton[5], Jamie Wilson[6], Andy Ridgwell[7]

The end-Cretaceous bolide impact triggered the devastation of marine ecosystems. However, the specific kill mechanism(s) are still debated, and how primary production subsequently recovered remains elusive. We used marine plankton microfossils and eco-evolutionary modeling to determine strategies for survival and recovery, finding that widespread phagotrophy (prey ingestion) was fundamental to plankton surviving the impact and also for the subsequent reestablishment of primary production. Ecological selectivity points to extreme post-impact light inhibition as the principal kill mechanism, with the marine food chain temporarily reset to a bacteria-dominated state. Subsequently, in a sunlit ocean inhabited by only rare survivor grazers but abundant small prey, it was mixotrophic nutrition (autotrophy and heterotrophy) and increasing cell sizes that enabled the eventual reestablishment of marine food webs some 2 million years later.

INTRODUCTION

The asteroid impact at the Cretaceous-Paleogene (K/Pg) boundary 66 million years (Ma) ago triggered a cascading mass extinction through the entirety of the global food web that occurred in a geological instant (days to years) (*1*–*3*). From giant marine reptiles to sharks and ammonites, down to microscopic plankton, most marine vertebrates and invertebrates were eliminated, leaving an ocean bereft of diversity and biomass (*1*, *4*). The precise kill mechanism(s) associated with the impact are still debated, but an array of environmental changes would have accompanied the release of impact-related debris, aerosols, and/or soot, with models predicting varying degrees of darkness, cooling, and acidification over days and years (*5*–*7*). One of the key open ocean primary producers of the Cretaceous was the coccolithophores: An extant group of haptophyte algae characterized by calcareous cell-wall coverings (coccospheres) and a unique flagellum-like organelle called a haptonema. Coccolithophores were almost entirely eradicated (>90% species extinction) at the K/Pg boundary (*8*, *9*). Their diversity loss and post-boundary near-absence in deep-sea sediments, together with geochemical evidence for shutdown of organic carbon export to the seafloor (the biological pump), are all indicators of the devastating disruption of primary production (*4*, *9*–*11*) and the consequential cascading extinctions that removed higher trophic levels (*4*, *10*, *11*). Precisely when primary production recovered and at what strength is currently uncertain, but the survival of some deep-sea benthos and limited biomarker evidence suggest that at least partial recovery occurred quickly (years to tens of years), with ubiquitous, prokaryotic cyanobacteria likely being the main primary producers as light levels improved (*4*, *12*–*14*).

The return of eukaryotic plankton would have been critical in facilitating the reestablishment of complex food chains from the bottom-up and for restoring the biological pump (*9*)—Several coastal eukaryotic plankton groups, especially dinoflagellates and diatoms, may have suffered less catastrophic extinction than the

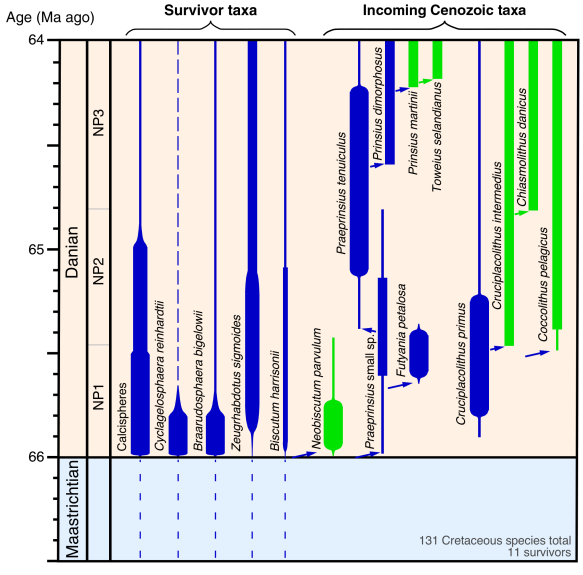

Fig. 1. Stratigraphic distribution and trophic strategy of selected survivor and incoming nannoplankton taxa. Important survivor taxa are indicated on the left, and incoming species are indicated on the right with an indication of principal trophic mode [based on our assessments, (*24*), Table 1, and table S1]: mixotrophs in blue and autotrophs in green. Bar thickness is a qualitative indication of abundance, with the broadest bars showing acme abundances. Dashed lines indicate dominantly coastal or neritic distributions. Close phylogenetic relationships are shown by arrows. The ancestry of *Cruciplacolithus* is uncertain but may lie with the Biscutaceae. The nannoplankton data are primarily from our work but are largely consistent with published sources. NP, nannofossil biozone.

[1]Ocean and Earth Science, National Oceanography Centre, Southampton, University of Southampton, Southampton SO14 3ZH, UK. [2]Department of Earth Sciences, University College London, Gower Street, London WC1E 6BT, UK. [3]University of Gibraltar, Europa Point Campus, Gibraltar GX11 1AA, Gibraltar. [4]Ecole Normale Supérieure, PSL Research University, Institut de Biologie de l'Ecole Normale Supérieure (IBENS), Centre National de la Recherche Scientifique (CNRS) Unité Mixte de Recherche (UMR) 8197, Institut National de la Santé et de la Recherche Médicale (INSERM) U1024, 46 rue d'Ulm, F-75005 Paris, France. [5]The Lyell Centre for Earth and Marine Science and Technology, Heriot-Watt University, Edinburgh EH14 4AS, UK. [6]School of Geographical Sciences, University of Bristol, University Road, Bristol BS8 1SS, UK. [7]Earth and Planetary Sciences, University of California at Riverside, Riverside, CA 92521, USA.
*Corresponding author. Email: samantha.gibbs@noc.soton.ac.uk
†These authors contributed equally to this work.
‡Present address: Department of Earth Sciences, University of Oxford, South Parks Road, Oxford OX1 3AN, UK.

Table 1. Description, images, and ecology of nannoplankton taxa that are found as fossils in the Upper Cretaceous and survive the K/Pg mass extinction event. Coccosphere morphology is based on observation of preserved coccospheres except for *Calciosolenia*, which is based on the shape of the coccosphere in its living species. *Neocrepidolithus*, *Zeugrhabdotus*, *Lapideacassis*, and *Octolithus* are extinct taxa that have never been observed as intact coccospheres, but modern coccospheres of taxa with the same coccolith morphology (muroliths) as *Neocrepidolithus* and *Zeugrhabdotus* tend to have very high lith numbers and are typically found in more coastal areas. Information about living relatives can be found summarized in (*27*). Survival mechanism listed here is based on whether we consider that their ecology and/or coccosphere morphology points to potential mixotrophy. *Markalius* is the most ambiguous as they form typical placolith-morphology coccospheres that are spherical and have low C_n (number of coccoliths per coccosphere) and no openings. Source of SEM images: (*27*, *38*, *73*). The coccosphere next to *Octolithus* is a representative modern holococcolith coccosphere (*27*). SEM images are not to the same scale.

Survivor taxon and family	Coccosphere morphology	Paleobiogeography, living relative ecology	Survival mechanism(s)	Rationale
Braarudosphaera, Braarudosphaeraceae 	Imperforate dodecahedron in calcified phase (seen as fossils)	Coastal, coastal	Mixotrophy in dominant, noncalcified motile phase, possible resting cyst (the dodecahedron coccosphere), endosymbiotic cyanobacteria.	*Coastal distribution, mixotrophy, and dominance of motile phase have been documented (*68*, *69*), and calcified resting cyst stage is highly likely (Hagino pers. comm.). In addition, extant forms have endosymbiotic cyanobacteria (*70*).
Cyclagelosphaera, Watznaueriaceae 	Imperforate sphere	Coastal, coastal	Coastal mixotrophy, existed in dominant motile (noncalcified) phase?	†Coccolith-bearing phase shows no evidence for a flagellar opening, but modern dominant phase (noncalcified) is likely motile, and coastal ecology points to mixotrophy (*68*).
Biscutum, Biscutaceae 	Ellipsoidal to cylindrical with possible flagellar opening	Coastal, coastal	Coastal mixotrophy.	Ellipsoidal coccosphere with potential flagellar openings plus coastal/near-shore ecology (*19*, *71*) points to mixotrophic capacity.
Markalius, *Incertae sedis* 	Imperforate sphere	Coastal, extinct	Coastal mixotrophy?	No evidence for a flagellar opening but coastal ecology could point to mixotrophic capacity. Similar to *Cyclagelosphaera*?
Neocrepidolithus, Chiastozygaceae 	Unknown, similar to modern murolith spheres with high C_n?	Coastal, extinct	Mixotrophy?	Coastal ecology and potentially high C_n could point to mixotrophic capacity. Many modern coastal murolith species are flagellate [see (*27*)].
Zeugrhabdotus Chiastozygaceae 	Unknown, similar to modern murolith spheres with high C_n?	Coastal, extinct	Mixotrophy?	High latitude and coastal ecology (*19*), plus potentially high C_n could point to mixotrophic capacity. Many modern coastal murolith species are flagellate [see (*27*)].
Lapideacassis, Lapideacassaceae 	Unknown	Coastal, extinct	Mixotrophy?	Unusual coccolith morphology and atypically restricted coastal ecology point to mixotrophic capacity.
Calciosolenia, Calciosoleniaceae 	Fusiform with flagellar opening	Coastal, coastal	Mixotrophy	Strongly fusiform coccosphere with flagellar openings plus coastal ecology (*72*) points to mixotrophic capacity.
Goniolithus, Goniolithaceae 	Imperforate dodecahedron	Coastal, extinct	Resting cyst and/or mixotrophy?	Similar morphology to *Braarudosphaera* could suggest similar ecology, but atypical restricted coastal ecology also points to mixotrophic capacity.
Octolithus, holococcolith 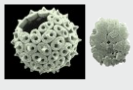	Holococcolith, unknown sphere	Coastal, extinct	Mixotrophy	Living holococcolith-phase coccolithophores are typically flagellate‡, and coastal ecology also points to mixotrophic capacity

*Modern *Braarudosphaera* is highly anomalous among coccolithophores in having a possible resting phase and endosymbionts. †*Cyclagelosphaera*, while exhibiting a typical imperforate coccosphere in its calcifying phase, again appears highly anomalous as modern observations indicate that it is coastal and only exists for a short time in this life-cycle phase (*68*). ‡Holococcoliths are specific to the haploid phase of coccolithophores that is characteristically motile (*25*).

open ocean plankton (*15*, *16*), and this is ascribed to greater trophic flexibility and their ability to form resting cysts with long dormancy potential (e.g., 100 years or more) [see (*17*)]. However, neither of these plankton groups was abundant in the Late Cretaceous open ocean nor proliferated away from the shelves in the aftermath of the mass extinction. Instead, we see recolonization and rapid rise to dominance of the coccolithophores once more, raising the question: How did a nominally obligate-phototrophic plankton group not only survive the post-impact darkness but also rapidly reestablish their dominance across the largest ecosystem on Earth? Here, we use exquisitely preserved plankton microfossil records in conjunction with a new eco-evolutionary model to elucidate the ecological strategies that characterize the survivors of the K/Pg event and the successful groups that rapidly repopulated the oceans. Our fossil evidence allows us to identify an innovative ecological strategy in the post-extinction plankton communities, and our model outputs provide a theoretical explanation for this unique natural experiment in ocean ecosystem reconstruction.

RESULTS AND DISCUSSION

Fossil nannoplankton evidence for global mixotrophy

The fossil record of calcareous nannoplankton (predominantly coccolithophores) reveals devastating losses of open ocean eukaryotic primary producers at the K/Pg, followed by rapid recolonization of the oceans by a succession of dominating species (so-called "acmes"; fig. S1), that included Cretaceous holdover "survivor" taxa and new "incoming," descendant groups (Fig. 1) (*8*, *9*, *18*, *19*). The dominant extant and, by analogy, fossil nannoplankton species are nonmotile, open ocean phytoplankton with photosynthesis their principal trophic mode. Coccolithophores have complex haplodiplontic life cycles with both haploid and diploid phases capable of independent asexual reproduction (*20*, *21*). Diploid cells are predominantly (although not exclusively) nonmotile, and these forms with imperforate coccospheres represent most cells in pelagic coccolithophore communities. Calcified haploid cells are typically motile and comprise less than 1% of coccolithophore cells in the open ocean (*21*–*23*).

Our first key finding here is that most of the incoming, post-extinction acme taxa (*Praeprinsius*, *Futyania*, and early *Prinsius*) have distinct openings in their fossilized coccospheres (Fig. 2, table S1, and fig. S2, A and B) (*24*). These perforate coccospheres are found across all the oceanographic settings we studied, from shelf to open ocean, and are formed from coccoliths (heterococcoliths) that characterize the diploid phase in these taxa. These openings indicate the presence of flagella in life that would have allowed for motility (Fig. 2F), an observation that aligns these fossil taxa most closely with modern motile coccolithophores and other haptophytes [see (*25*, *26*) and images in (*27*)] that are typically more diverse in shelf and coastal areas [e.g., (*22*, *23*)]. Modern motile haptophytes have two flagella and a haptonema (Fig. 2F) that act together to capture and ingest prey particles, such as bacteria and small algae (*26*, *20*, *28*). Motility can therefore be considered a prerequisite for phagotrophy (*20*, *26*). Coccolithophores also have chloroplasts, and therefore, phagotrophy, when executed, makes these cells mixotrophic, i.e.,

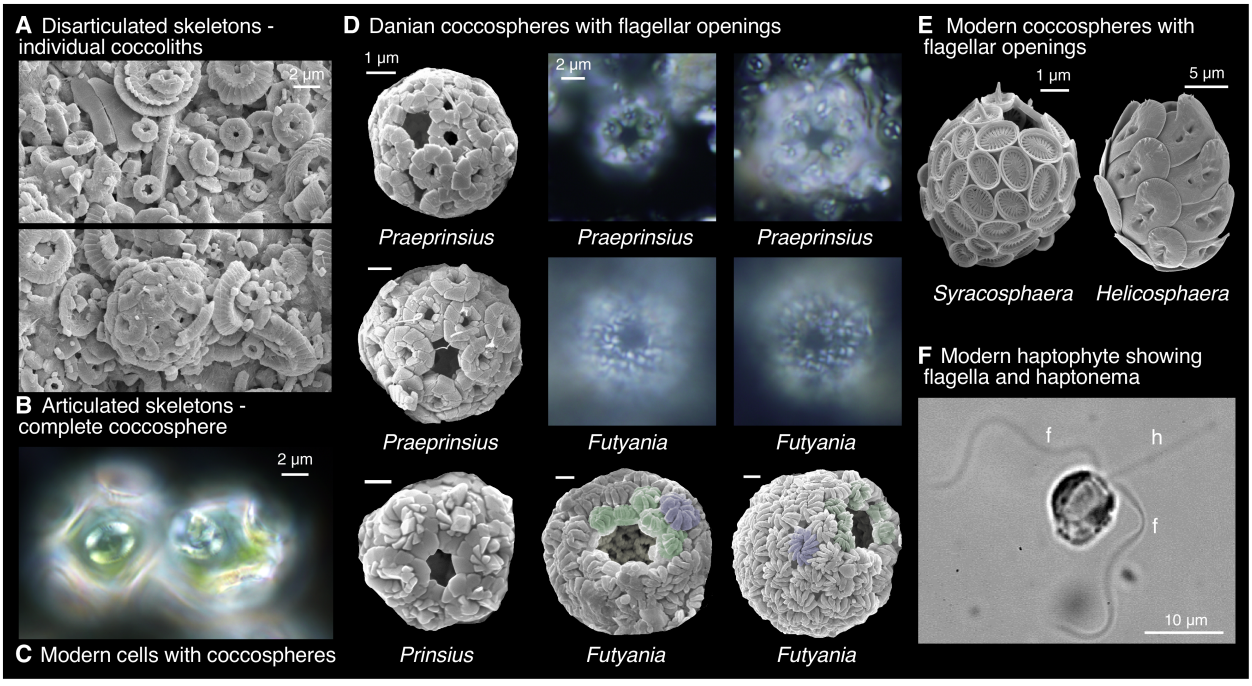

Fig. 2. Modern and fossil coccolithophore cell wall coverings. (**A** and **B**) Scanning electron microscopy (SEM) image showing disarticulated coccoliths (A) and complete coccosphere (B) [Danian, Newfoundland Ridge, Integrated Ocean Drilling Program (IODP) Site 1407 sample 1407A-23-2, 50 cm]. (**C**) Light microscope (LM) image showing modern coccospheres of *Coccolithus* in culture as an example of nonflagellate, diploid, heterococcolith coccospheres. Cells from culture experiments performed in (*58*) using a North Atlantic open ocean isolate RCC1197. (**D**) SEM and LM images of complete Danian diploid, heterococcolith coccospheres with flagellar openings (additional examples in fig. S2). The SEM *Praeprinsius* are from Newfoundland Ridge (upper specimen from sample 1407C-20-4, 125 cm, and lower from sample 1407A-23-2, 35 cm). *Prinsius* from a North Sea well sample (see table S2) and both *Futyania* are from Blake Nose sample 1049C-8-4, 38 cm. The LM images of *Praeprinsius* are from 1407A-23-2, 50 cm, and those of *Futyania* are from 1407C-20-4, 125 cm. Modified circumflagellar coccoliths are shown in green for *Futyania*. (**E**) Modern coccospheres with flagellar openings [from (*27*)]. (**F**) LM image showing cell (*Prymnesium parvum*) with flagella (f) and haptonema (h) [from (*26*)].

able to acquire essential nutrients and carbon from prey ingestion and photosynthesis.

Second, we found that the Cretaceous nannoplankton taxa that survived the mass extinction event either have morphologies indicative of phagotrophy (i.e., flagellar openings) or typically have inhabited shelf or coastal regions where today mixotrophic haptophytes are predominantly found (see Table 1) (*22*, *23*, *29*). This potential capacity for mixotrophy in the survivors suggests that nannoplankton endured the mass extinction event using phagotrophy, likely feeding on bacteria and/or organic matter washed in from rivers and tsunamis (*3*, *30*) during the post-impact blackout that may have persisted from weeks to 2 years (*5*, *6*).

Next, we analyzed nannoplankton population data across the 4 Ma that follow the K/Pg at widely separated sites in the central Pacific [Ocean Drilling Program (ODP) Site 1209, data from (*9*)], North Atlantic, and South Atlantic oceans [Integrated ODP (IODP) Sites 1403 and 1407 and ODP Site 1262, data here; figs. S1, S3, and S4], calculating the proportion of the community that exhibit phagotrophic morphology (including both survivors and the new incoming taxa) (*24*). The data show a rapid increase in mixotroph abundance over the first few 100 ka to a sustained peak of 70 to 100% of the fossil cells (Fig. 3). This reflects the relative contributions of early, survivor acmes (*Braarudosphaera* and *Cyclagelosphaera*) and incoming mixotrophic taxa (*Praeprinsius*, small *Cruciplacolithus*, and *Futyania*), together with the incoming *Neobiscutum* (which shows no obvious morphological evidence for phagotrophy) (fig. S1). Around 500 ka after the K/Pg event, there is an increase in new, descendant taxa within the main lineages that show no evidence of flagellar openings (*Coccolithus pelagicus* and large *Cruciplacolithus* spp.), reflecting the rising influence of photoautotrophic strategies (Fig. 3 and fig. S1). After 64.2 Ma, ~1.8 Ma after the event, the levels of mixotrophic cells decline to a consistently low background level (Fig. 3), which is coincident with the cessation of the acme succession and also full recovery of the biological pump (*9*, *10*).

Our data indicate that mixotrophic nannoplankton taxa preferentially survived the mass extinction and, once light levels were restored, largely dominated the communities across the following million years. Surviving Cretaceous taxa, previously restricted to shelf areas (see Table 1) (*19*), expanded their biogeographic ranges into the open ocean and were joined and then rapidly overtaken, by newly evolving photoautotrophic and mixotrophic taxa. The dominance of mixotrophic coccolithophores in the Danian open ocean is highly anomalous compared with the modern or any other interval of the Cenozoic. While the rapid global recolonization of the oceans by mixotrophs may, in part, reflect an ecological "bottleneck" at the mass extinction [i.e., mixotrophs survived and then seeded recolonization, e.g., see (*31*)], it does not explain why mixotrophy persisted for so long. We therefore also need to explore why mixotrophy conveyed such a notable ecological advantage to these early (re-)colonizers.

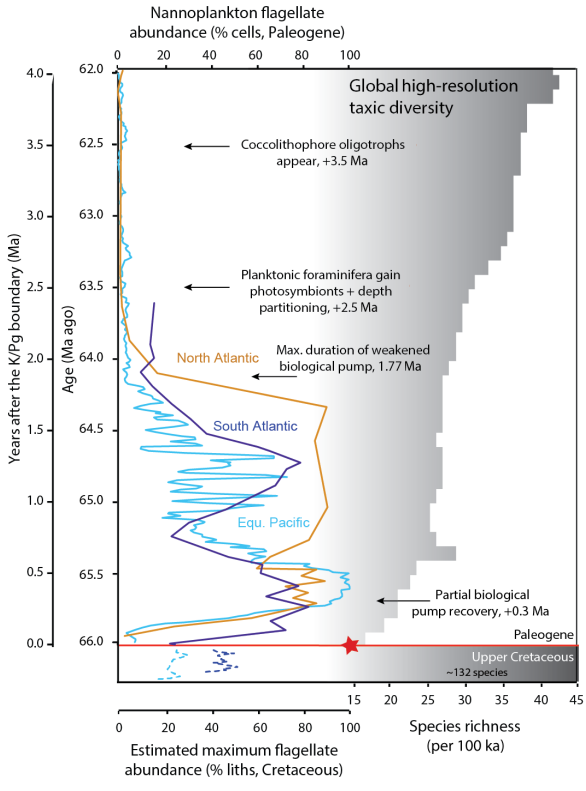

Fig. 3. Fossil nannoplankton abundance of flagellate cells and species richness. On the left is the percent flagellate cells (*24*) from sites in the South Atlantic (ODP Site 1262, dark blue), North Atlantic (IODP Sites 1403 and 1407, brown), and the palaeosubequatorial Pacific (ODP Sites 1209 and 1210 and DSDP Site 577, light blue). The percent flagellate cell abundances for the Upper Cretaceous (dashed blue lines) are shown as the percentage of coccolithophores of unknown ecology, of which there may be some flagellate taxa (*24*), providing us with a maximum possible estimate. The position of the red star indicates our suggestion that all taxa that survived across the K/Pg boundary were capable of phagotrophy. Paired-sample *t* tests, comparing the percentage of flagellate cells between the early Danian (up to 64.2 Ma) and both the Late Cretaceous and the later Danian (after 64.2 Ma), indicate significant differences between communities in all cases (see table S3). On the right is the high-resolution (number of species present per 100 ka) fossil calcareous nannoplankton species richness (*10*). Milestones in ecosystem recovery in the post-extinction ocean are indicated (*10*, *11*). Paleogene data are shown against age. The Cretaceous data are a representative uppermost portion, with no high-resolution age assignment (*24*).

Eco-evolutionary modeling of early recovery plankton communities

Here, we turned to a new eco-evolutionary model to better understand the role of mixotrophy, allowing us to explore ab initio plankton recovery in a post-extinction ocean. We focus on a model experiment in which we seed empty, sunlit, and nutrient-replete seawater with small photoautotrophic cells and then run it forward in time letting the ecology "evolve" (*24*). These cells are referred to as "autotrophic," but they have the capacity to adopt mixotrophy and heterotrophy without the need to completely evolve new machinery. They do, however, require "evolution" to produce new genotypes or species that exhibit different trophic strategies. Because the model applies a simplified "trait diffusion" approach to evolution, it means that the mutation and evolution proceed much faster in the model than in the data. Our model initial state hence represents a highly idealized reconstruction of the post-extinction open ocean, mimicking the earliest phase of recovery after post-extinction darkness, where primary production has resumed but grazers remain absent.

There are key features that are evident in both model outputs and fossil data. The model output first shows a succession of abundance maxima of closely related genotypes, each temporarily proving to be the most successful and dominant taxon (fig. S4). This is notably similar to the fossil nannoplankton acme patterns (figs. S1 and S4). The model also shows a clear prevalence for mixotrophy emerging in the early to mid-acme phase (blue-green to pale pink

colors in Fig. 4), and, likewise, we observe mixotrophy as the dominant ecological strategy in the nannoplankton fossils for much of the first 2 Ma after the K/Pg event (Fig. 3). In addition, the model shows an increasing cell size trend, which we also see across the nannoplankton community [see (*9*)] and within individual taxa, during this interval (fig. S5). This dynamic, succession phase then stabilizes abruptly in the model, shifting to a more diverse, equilibrium-state community with a broader cell size spectrum (Fig. 4 and fig. S4). This is echoed in the fossil communities, which shift to a stable background state at ~+1.8 Ma, as diversity and cell size ranges increase [Fig. 3 and see (*9*)]. Last, the model shows mixotrophic acme taxa giving rise to obligate photoautotrophic descendants (as well as obligate heterotrophs) (Fig. 4 and fig. S4), a trend that is also evident in the fossil successions, as the dominant lineages give rise to new coccosphere geometries with no flagellar openings (*Praeprinsius* to *Prinsius-Toweius* and *Cruciplacolithus* to *Coccolithus*) (Figs. 1 and 3).

Examining the model's fitness landscape allows us to explore the key mechanisms driving the evolutionary recovery (Fig. 5). A fitness landscape essentially maps the competitive ability of all possible phenotypes as a function of their contemporary environment. In each case, the height of the landscape (here shown as colors) corresponds to potential net population growth rate or "fitness." In our example, peaks (red) in the landscape correspond to areas where a population would successfully grow, and blue areas mark where cells are not viable. Superimposed on this landscape are model populations that, through time, effectively climb the fitness landscape. During the initial phase (Fig. 5) and in the absence of larger predators, there is prolific growth of the small photoautotrophic community. The emergence of this underexploited prey population creates a large peak in the fitness landscape, representing a huge empty niche for potential predators. This niche is progressively occupied in the subsequent time slices by a rapid evolutionary succession of larger and increasingly heterotrophic species. Across this transient interval, mixotrophy allows small phototrophs to access the newly emergent niche associated with the underexploited prey population. As recovery continues, the adapting community is subjected to opposing evolutionary factors, with smaller size conveying advantage to photoautotrophs in competition for essential resources (light and nutrients) and larger size enabling grazing and access to the abundant prey community. These opposing factors create an evolutionary branching point. One lineage continues toward a more heterotrophic lifestyle (Figs. 4 and 5), but the transitory advantage of mixotrophy among smaller cells mostly disappears, driving them to revert to a photoautotrophic strategy. Ultimately, the system reaches

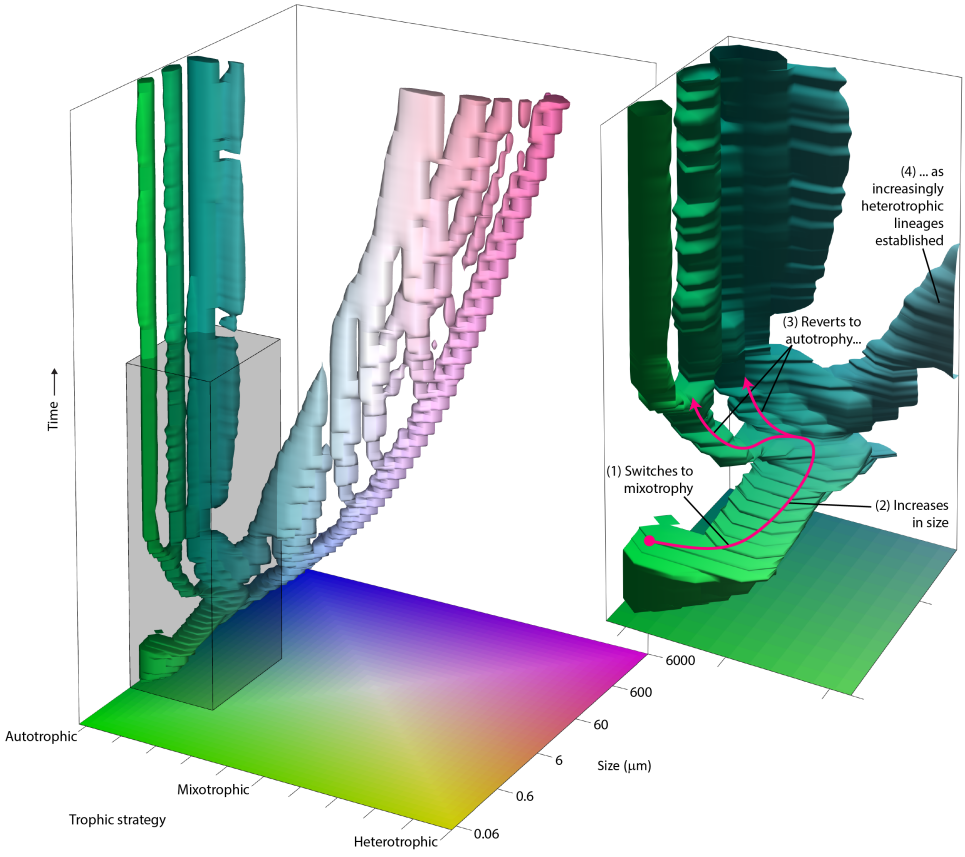

Fig. 4. Evolution of traits in the model plankton community. The tree structure describes the evolutionary development of the community, with the trajectory of each branch describing changes in the trophic strategy and size of an individual population through time. With time progressing from the bottom up, evolutionary changes to traits are represented by changes in the horizontal position (and color) of its respective branch in the tree. Speciation occurs when one branch divides into two. The inset panel shows a more detailed view of the tree for the region bounded by the gray box, broadly corresponding with the cell size range of coccolithophores. The shape of the tree is technically defined by a three-dimensional surface contour (trophic strategy, size, and time) inside which population biomass exceeds 0.01 mmol N^{-1} m^{-3}. Note that mutation and evolution proceed much faster in the model because the model applies a simplified trait diffusion approach to evolution (*24*).

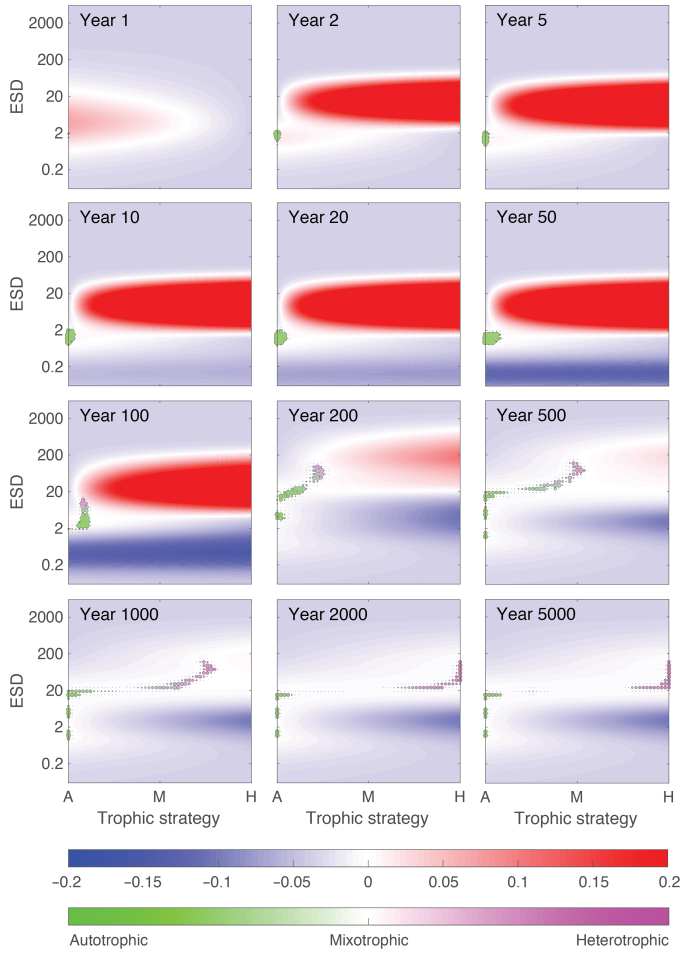

Fig. 5. Evolution of the plankton community and the fitness landscape through time. Each panel represents two-dimensional "trait space" of trophic strategy and equivalent spherical diameter (ESD; in micrometers). Background colors (red to blue) describe changes in fitness landscape through time, with height equivalent to biomass-specific net population growth rate. Dots indicate extant populations, with area proportional to population size and color (green to magenta) indicating the balance of autotrophic and heterotrophic nutrition. At year 1, biomass is low and inorganic resources are high, and we see a peak in the fitness landscape centered on fast growing autotrophic cells. By year 2, the population has increased, and a new peak in the fitness landscape has emerged for larger and more heterotrophic traits driven by this potential prey. Over the next 100 years or so, the initial population adapts toward the new fitness landscape peak, with small mixotrophs coexisting with the initial photoautotrophic population. After approximately 100 years, the community has gained sufficient size diversity to begin showing predator-prey dynamics. The evolving community then branches, heading toward the stable coexistence of small phytoplankton, intermediate mixotrophs, and larger zooplankton. At year 5000, it can be seen that there are no remaining positive regions of the fitness landscape, indicative of a community at an ecological and evolutionary equilibrium.

a stable state characterized by the coexistence of photoautotrophs, mixotrophs, and heterotrophs. We are not arguing that the model captures a real-world picture of ecosystem evolution, but both fossil data and model outputs indicate that mixotrophic strategies, acme successions, and cell size increases are key features of recovering plankton communities after a mass extinction level event, with mixotrophic nutrition providing the mechanism by which predation and top-down controls are reestablished in the recovering food web.

Implications

Our evidence for pervasive phagotrophy in open ocean eukaryotic "autotrophic" survivors and recolonizers explains how a remnant of the dominant Cretaceous primary producers survived the K/Pg mass extinction. Alongside supporting eco-evolutionary model results, this indicates that mixotrophy in recovering communities is a critical and predictable feature of ecosystem reconstruction. We conclude that the protracted darkness of the impact winter acted as a near-instantaneous state-change filter on the open ocean, stripping out almost all plankton that lacked a capacity for phagotrophy. This filter likely extended across the entire diversity of marine plankton as virtually all extant eukaryotic photosynthetic plankton (e.g., haptophytes, dinoflagellates, raphidophytes, and euglenophytes) still exhibit some heterotrophic capacity [e.g., see (*32*–*34*)]. While global cooling and ocean acidification have also been proposed as primary or accessory K/Pg kill mechanisms (*5*, *7*), the selectivity seen across the survivor and repopulating plankton groups can only be fully explained by the impact of darkness, i.e., preferential removal of open ocean photoautotrophs but survival of mixotrophic counterparts. Although high extinction rates across the calcifying plankton could implicate acidification (*7*), all three major groups survived (nannoplankton, calcareous dinoflagellates, and planktonic foraminifera). Furthermore, we see that survivorship was spread across eight families in the nannoplankton, with no indication of selectivity bias in degree or style of calcification, i.e., a range of morphologies survived, including both lightly and heavily calcified forms (Table 1).

Together, the selective loss of key open ocean photoautotrophs and prevalence of phagotophy in the surviving algal groups suggests that primary production was drastically disrupted by the K/Pg bolide impact, pointing to a complete cessation of all marine photosynthesis during peak impact darkness. If not for the nutritional flexibility of the eukaryotic plankton that were able to use antecedent hunting strategies, then the K/Pg impact could have resulted in a resetting of marine ecosystems back to a principally prokaryotic state. The K/Pg mass extinction event is therefore distinct from all other mass extinction events that have shaped the history of life in both its rapidity, related to an instantaneous impact event, and its darkness kill mechanism, which fundamentally disrupted the base of the food chain. In this sense, the K/Pg could be regarded as more "severe" than the end-Permian and other first-order events, where extinctions occurred across protracted time intervals of tens of thousands to millions of years (*35*, *36*). These events were predominantly associated with volcanogenically induced climate change triggers and a broader range of kill mechanisms, including global warming, marine anoxia, and ozone depletion (*36*). Arguably, the K/Pg boundary event represents the only truly geologically instantaneous mass extinction.

MATERIALS AND METHODS

Data, sites, and material

The data and observations we present here come from both (i) whole coccospheres (intact fossil cell coverings) that allow us to determine which taxa have flagellar openings (see below) and (ii) loose coccoliths (i.e., disarticulated coccospheres) that provide detailed abundance, size, and diversity data through time and between different locations (see table S4). We show data that include coccolith abundance data, morphometric data from individual coccoliths,

and measurements from coccospheres, all differentiated by taxon. We used a global array of sites, spanning a range of latitudes and oceanographic settings (shelf, slope, and open ocean) (fig. S3 and tables S1 and S2), including ODP Site 1209 (Shatsky Rise in the northwest Pacific Ocean), ODP Site 1262 (Walvis Ridge in the South Atlantic Ocean), IODP Sites 1403 and 1407 (Newfoundland Ridge in the North Atlantic Ocean), El Kef outcrop (onshore Tunisia), ODP Site 1049 (Blake Nose, North Atlantic Ocean), and ODP Site 690 (Maud Rise, Southern Ocean), detailed in table S2. This range of observations is extended further by reference to previously published scanning electron microscopy (SEM) images in which we have identified coccosphere openings. These include coccospheres from West Alabama (USA) (*37*), Geulhemmerberg (Netherlands) (*38*), Deep Sea Drilling Project (DSDP) Site 356 Sao Paulo Plateau (South Atlantic Ocean) (*39*), and ODP Site 738, Kerguelen Plateau (Indian Ocean sector of the Southern Ocean) (*40*). Because there may be preservational and algal community differences between open ocean and near-shore regions, this site selection allowed us to determine the global open ocean picture of recolonization and whether shelf to off-shelf differences may have existed. Most of the material displayed good to excellent preservation of nannofossils except for ODP Sites 1209 and 1210 and ODP Site 1262 that show moderate to good preservation, i.e., some etching/dissolution and/or overgrowth of nannofossils [following definitions of (*41*)], typical of carbonate-rich deep-sea sediments. Excellent preservation at the other sites is identified by little etching or overgrowth and the presence of features indicative of "exceptional" preservation (*42*), including minute coccoliths, delicate structures, and intact coccospheres. Preservation of each sample was assessed qualitatively using preservation criteria based on levels of etching and overgrowth. Assessment was based on appearance under light microscope (LM) observation and using high-resolution images from SEM.

Sample preparation

Samples were prepared for LM observation, using standard smear slide techniques (*41*) and SEM observation, using both smear slide and rock-chip preparations (*43*). Smear slides were observed under transmitted LM in cross-polarized and phase-contrast light at ×1000. In SEM, we used freshly cleaved untreated rock-chip preparations allowing the observation of coccolithophore remains in situ, embedded in clay matrix. This minimizes any disturbance that may physically disrupt the articulated fossils and may allow determination of original export pathways, for example, through observation of fecal pellets or concentrations. We also used smear slide preparations in SEM to enable freeing of the coccospheres from the clay matrix.

Morphological evidence for mixotrophy

The preservation of complete fossil cell-wall coverings (coccospheres) at multiple sites (Fig. 2, fig. S2, and tables S1 and S2) allowed us to search for diagnostic indicators of specific ecological strategies. We imaged and recorded several thousand coccospheres of the taxa that rose to dominance sequentially, so-called acmes (fig. S1), from throughout the first 4 Ma after the K/Pg event from LM and SEM (table S1). The main indicator of mixotrophy here is a clearly defined, consistently sized hole in the coccosphere, representing a flagellar opening. In *Praeprinsius*, *Futyania*, and early *Prinsius*, these holes were present in mass occurrences of tens of thousands of specimens in each sample preparation, across sites situated both close to shore and in the open ocean, and from low to high latitudes (tables S1 and S2). In *Futyania*, these holes were surrounded by modified coccoliths [circumflagellar liths; Fig. 2 and fig. S2A; e.g., (*27*, *44*)], providing unequivocal evidence that these "holes" were not a result of postmortem coccolith loss. We observed these openings under LM (e.g., Fig. 2 and fig. S2B) and confirmed their presence using SEM (e.g., Fig. 2D and fig. S2A). We then systematically quantified and imaged 100 to 200 coccosphere specimens per site mainly under LM of all of the acme taxa—*Praeprinsius*, *Futyania*, *Prinsius*, *Coccolithus*, *Cruciplacolithus*, and *Neobiscutum*—recording the presence or absence of coccosphere openings (table S1). Note that all coccospheres we recorded were from heterococcolith-bearing coccolithophores, indicating the diploid life-cycle phase in these taxa. We were able to determine the likelihood that coccosphere openings were present in all fossil individuals for each taxon that exhibited holes, by calculating the spherical area observed under LM, given the obfuscation of the equatorial region. On the basis of a conservative estimate that the observation of spheres via LM allows us to clearly see from the pole of each coccosphere to about 65° in the upper and lower hemispheres, this would correspond to 60% of the surface area. Therefore, if ~60% or more of the specimens exhibit holes, then we can to be confident that all the spheres of that taxon in that population have holes (fig. S6). We also explored the morphology of the spheres under SEM, but because only one hemisphere can be observed using this method and the equatorial region is again typically obscured, the proportion of specimens with observable holes will be less than for LM observation, potentially half, i.e., only 30% of the coccosphere area. Table S1 shows the percentage of each taxa exhibiting holes and highlights in bold where the values exceed these threshold percentages of 60% for LM and 30% for SEM. There is a variation in the percentage of individuals exhibiting holes across the samples and sites, but the average percentage occurrences (under LM) for *Praeprinsius* and *Futyania* are close to this 60% value (58 and 66%, respectively), indicating that it is likely that most, if not all, individuals in the fossil populations of these taxa have coccosphere openings.

For the purposes of calculating percent "mixotrophs/flagellates" and assigning ecology for Fig. 3 and fig. S4, we considered *Praeprinsius*, *Futyania*, and early *Prinsius* as being flagellate (based on the presence of coccosphere openings described above). We also added small *Cruciplacolithus* to this group of mixotrophs. This is because the "flagellate" acme taxa coccospheres also exhibit unusual architectures with large numbers of very small coccoliths surrounding a relatively large cell, consistent with the needs of a mixotrophic cell to accommodate the apparatus for phagotrophy (a food vacuole), photosynthesis (chloroplasts), and coccolith production (coccolith-forming vesicles). Coccolith formation in placolith-bearing coccolithophores occurs inside the cell, and the coccoliths are extruded fully formed and at their final size. Therefore, smaller coccolith-forming vesicles (and smaller associated coccoliths) would be advantageous, or a necessity, in small cells accommodating other large organelles, such as a food vacuoles. *Cruciplacolithus primus* has this architecture, and its living relative, *Cruciplacolithis neohelis*, has coastal ecology and produces motile cells (*45*). Calcareous dinocysts were also included because their modern ecology indicates a capacity for heterotrophy (*46*, *47*). In addition, we included holococcoliths (predominantly *Zygrhablithus*) in the "percent mixotrophs" together with the survivor taxa that exhibit architectures consistent with mixotrophy (Table 1), but these make up only a small proportion of total nannofossil abundance.

Abundance data

Raw coccolith abundance data from Shatsky Rise, Walvis Ridge, and Newfoundland Rise—in the Pacific and South and North Atlantic oceans (illustrated in part in fig. S1), respectively—were used to calculate the relative proportion of flagellate/mixotrophic taxon abundance versus nonflagellate/autotrophic taxon abundance through time. Taxon abundance data were generated from LM smear slides with data collection following the same count and taxonomic protocols of (*48*) across all three sections. Danian abundance data from ODP Site 1209 samples are published in (*9*) except that *Cruciplacolithus* data have herein been separated into small and large forms based on new coccolith measurement data (see below). The Danian Walvis Ridge and Newfoundland data are new herein. Counts from all sites were based on statistically significant counts of 500 to 1000 nannofossil liths per sample across a minimum of 10 fields of view, with taxonomy generally following (*27*, *49*, *50*). The assemblage data were counted to generic level, with some additional division into useful morphogroups [e.g., determined by genus and size, as detailed in (*9*)].

We wanted to document the trends in the incoming Danian taxa across three locations with the highest quality age control using the exact same taxonomic framework. The counts for both the Walvis Ridge and Shatsky Rise sites were made by the same nannofossil worker (S.A.A.), and the same taxonomy and approach was used by H.K., in collaboration with S.A.A., for Newfoundland. This was to minimize any inconsistencies in taxonomic attribution (which is a problem in this time interval) and to eliminate any false diachroneities that may arise from these inconsistences. ODP Site 1262 has a robust magnetostratigraphy and an orbitally tuned stratigraphy [(*51*) and updated in (*52*)] to which the ODP Site 1209 (which lacks reliable magnetostratigraphy) was correlated using tie points in the x-ray fluorescence core scanning and $\delta^{13}C$ data, as well as scrutiny of core images composites [(*51*–*53*) and summarized in (*9*)]. The IODP Sites 1403 and 1407 (Newfoundland Ridge) age models combine biostratigraphy from here and shipboard (*54*) with cyclostratigraphy (*2*).

To produce the percent flagellated data, the raw abundance data (fig. S1) in the form of loose coccolith data were recalculated to number of cells by dividing lith abundance by number of liths surrounding each cell—its C_n—which is taxon-specific (see "Biometric data" section below). Data file S1 provides the percent cellular abundances for Newfoundland Ridge, Walvis Ridge, and Shatsky Rise. Recalculating to number of cells provides a more biologically tangible abundance (rather than the number of disarticulated skeletal elements) and also removes the abundance bias toward taxa where there are a high number of coccoliths per cells. We then differentiated the cell abundances into flagellated and nonflagellated cells based on the coccosphere data and observations (detailed above) using the broad geographic array of observations of coccospheres. Hence, we do not need coccosphere data from all sites where we have abundance data (Shatsky Rise), rather, what we need is confidence that our conclusion that, for example, *Praeprinsius*, is flagellated wherever it occurs in the ocean.

For the Cretaceous datasets, details below, we could not convert coccolith abundance to cell abundances (because the information about C_n for Cretaceous taxa does not as yet exist). We therefore compared coccolith abundances for the statistical tests from both the Cretaceous and the Danian. The Cretaceous datasets are not on high-resolution age models, but we were able to select the uppermost approximately 2 Ma of the latest Cretaceous based on the biostratigraphy accompanying the data, selecting data falling within UC20b-d (*55*). High-resolution age models were not required for comparison within a paired *t* test (see below). Because we only have limited information about coccosphere morphology for Cretaceous taxa, we were not able to estimate "percent flagellate" forms, and so we calculated the percentage of definitely or almost certainly nonflagellate forms (e.g., *Watznaueria* and *Cribrosphaerella*) based on unpublished coccosphere observations and some published coccosphere images [e.g., (*38*)]. The remaining forms have unknown ecology, and we assume that there may be a proportion of these taxa that were flagellate. The percentage data given in Fig. 3 for the Cretaceous therefore represent the maximum possible percentage of flagellate forms and almost certainly would, in reality, represent a gross overestimate. In Fig. 3, we have shown the topmost part of these Cretaceous maximum flagellate datasets, spacing the data points closely and in stratigraphic order, but not against age. This is to allow for a broad comparison of the Cretaceous values with the Danian data.

Statistical analysis

We performed paired-sample *t* tests for comparison of percent flagellate cells in the early Danian (acme phase up to 64.20 Ma) with the Late Cretaceous and the later Danian (after 64.20 Ma) (table S3). The percent flagellate data within each stratigraphic block form the sample set that the test compares with other sets. The test outputs include the mean and SD of each of these sample sets. Available records for this purpose vary between sites. To compare the Paleogene estimates of flagellate abundance with preceding communities from the Cretaceous, we used existing datasets from Walvis Ridge [ODP Site 1262 (*56*)] and Shatsky Rise [ODP Site 1210 (*19*) and DSDP Site 577 (*57*)]. No equivalent Cretaceous record exists as yet for the Newfoundland Ridge sites (IODP Sites 1403 and 1407) or their vicinity. In table S3, note that the df (i.e., the sample size) varies between tests because we had to rely on the sampling resolution available for the data sources we used. This is why when a paired *t* test was performed between the early Danian and the Late Cretaceous versus the early Danian and the later Danian, the means of the early Danian block differ. The Late Cretaceous dataset is lower resolution than the Danian dataset, and therefore, we had to degrade the early Danian dataset (take every other sample rather than every sample) for the *t* test to ensure that the same number of samples was being compared.

Biometric data

Biometric data were collected from both disarticulated coccoliths and also fully articulated coccospheres. Routine data collection was made using LM with some additional measurement made on SEM images. For the *Praeprinsius* cell size data shown in fig. S5, measurements were collected from intact coccospheres from across the sites listed in table S1. Two images are taken from each coccosphere, one focused on the outer coccosphere circumference, providing the coccosphere and cell dimensions (the internal dimension representing the position of the original cell), and the second focused on the outer surface of the coccosphere, allowing the coccolith size to be measured (*58*). The number of coccoliths forming each coccosphere (C_n) was also recorded. Coccolith length plotted against cell size produces an equation that defines the regression allowing length to be converted into estimated cell size. With this information, we were able to use high-resolution *Praeprinsius* disarticulated coccolith measurements

(long axis of the distal shields) (*58*) collected here from Newfoundland and Shatsky Rise (>100 coccolith measurements per sample) to produce time series cell diameter histograms. Samples were integrated across 250-ka bins from 0 to 2 Ma after the extinction event (fig. S5). Images of coccospheres and disarticulated coccoliths were taken using the QCapture program, and lengths were measured using the ImageJ and CellD programs, measuring up to two decimal places. C_n data were also collected from additional Danian taxa, which, combined with data and estimates published in (*9*), allowed coccolith abundance data to be recalculated to cell abundance by dividing coccolith percent by C_n and then recalculating the resultant total number of cells to 100%. The taxon *Cruciplacolithus* was subdivided broadly according to coccolith size and high-resolution coccolith measurements from Shatsky Rise and Newfoundland Ridge, which allowed for quantitative differentiation of small and large forms. The coccolith length data highlight that populations are broadly bimodal with 6.5 μm defining the trough between modes and used here as our threshold between *Cruciplacolithus* large spp. and *Cruciplacolithus* small sp.

Eco-evolutionary modeling

We apply a "trait-based" modeling approach, which aims to represent the diversity of unicellular plankton in terms of two principal traits: organism size and "trophic strategy" (details in Supplementary Text). The simulated ecology conforms with our expectations based on related ecological (nonevolutionary) models (*59*–*61*) but with the recovery pathway notably constrained by the requirement for new populations to evolve from those already present. Allometric relationships with organism size explain most of observed variance in ecophysiological rates and predator-prey interactions (*62*–*64*), while the trophic trait parameter linearly scales resource acquisition traits along a continuous spectrum between strictly photoautotrophic phytoplankton and strictly organoheterotrophic zooplankton (*65*).

The evolutionary-ecosystem model represents a highly idealized abstraction of the post-extinction community, with the ecological and evolutionary emergence of a complex microbial food web from an initial low complexity state. It is seeded in a nutrient-replete state, mimicking the earliest recovery phase, where nutrients have built up because of reduced biological activity during the post-extinction darkness. These nutrients are rapidly drawn down to limiting concentrations after an initial ecological response, faster than the resolution of Fig. 4. Rather than entrain the interpretative complexities of running the model in a three-dimensional ocean circulation environment, we deliberately formulate the physical environment as a low volume (1 m^3) homogenous culture, with no spatial structure, environmental gradients, or boundaries to dispersal. The model includes 2601 possible plankton classes, each with a unique combination of the two principle traits (51 size classes and 51 trophic classes). All plankton classes are initialized with zero biomass, with the exception of a single population, which is seeded with a low initial biomass. From this initial biomass, extant populations grow (or die) as a function of both their phenotypic traits and their biotic and abiotic environment. At each time step, populations reproduce clonally, with a small fraction of their offspring diverted to populations with similar phenotypic traits (smaller or larger, more or less heterotrophic), in a process analogous to mutation. This creates the phenotypic variability on which "natural" selection can act, allowing new and better adapted phenotypes to emerge in the model community. Ecological dynamics determine the relative fitness of different phenotypes, with evolutionary adaptation occurring as the community shifts incrementally toward populations with better adapted traits. The time scales of change differ considerably between the data and the model because the model applies a simplified trait diffusion approach to evolution (*66*, *67*).

Given the abstractions in the model, the key process we aim to capture is not necessarily the precise time scales of recovery. The model and data diverge in this respect because the evolution in the trait diffusion approach we adopt (see the "Evolutionary dynamics" section in the Supplementary Materials) proceeds much faster than the rate of plankton mutation in the post-impact ocean. Rather, we aim to capture the constrained evolutionary trajectory through the represented trait space. That is, new phenotypes cannot emerge from nothing in previously unoccupied regions of the trait space. Instead, the community can only evolve through gradual changes to the existing phenotypes. It is this aspect of the model that underpins the transitions from small phototrophs to larger heterotrophic organisms via an intermediary mixotrophic stage.

SUPPLEMENTARY MATERIALS

Supplementary material for this article is available at http://advances.sciencemag.org/cgi/content/full/6/44/eabc9123/DC1

REFERENCES AND NOTES

1. P. Schulte, L. Alegret, I. Arenillas, J. A. Arz, P. J. Barton, P. R. Bown, T. J. Bralower, G. L. Christeson, P. Claeys, C. S. Cockell, G. S. Collins, A. Deutsch, T. J. Goldin, K. Goto, J. M. Grajales-Nishimura, R. A. F. Grieve, S. P. S. Gulick, K. R. Johnson, W. Kiessling, C. Koeberl, D. A. Kring, K. G. MacLeod, T. Matsui, J. Melosh, A. Montanari, J. V. Morgan, C. Neal, D. J. Nichols, R. D. Norris, E. Pierazzo, G. Ravizza, M. Rebolledo-Vieyra, W. U. Reimold, E. Robin, T. Salge, R. P. Speijer, A. R. Sweet, J. Urrutia-Fucugauchi, V. Vajda, M. T. Whalen, P. S. Willumsen, The Chicxulub asteroid impact and mass extinction at the Cretaceous-Paleogene boundary. *Science* **327**, 1214–1218 (2010).
2. P. M. Hull, A. Bornemann, D. E. Penman, M. J. Henehan, R. D. Norris, P. A. Wilson, P. Blum, L. Alegret, S. J. Batenburg, P. R. Bown, T. J. Bralower, C. Cournede, A. Deutsch, B. Donner, O. Friedrich, S. Jehle, H. Kim, D. Kroon, P. C. Lippert, D. Loroch, I. Moebius, K. Moriya, D. J. Peppe, G. E. Ravizza, U. Röhl, J. D. Schueth, J. Sepúlveda, P. F. Sexton, E. C. Sibert, K. K. Śliwińska, R. E. Summons, E. Thomas, T. Westerhold, J. H. Whiteside, T. Yamaguchi, J. C. Zachos, On impact and volcanism across the Cretaceous-Paleogene boundary. *Science* **367**, 266–272 (2020).
3. S. P. S. Gulick, T. J. Bralower, J. Ormö, B. Hall, K. Grice, B. Schaefer, S. Lyons, K. H. Freeman, J. V. Morgan, N. Artemieva, P. Kaskes, S. J. de Graaff, M. T. Whalen, G. S. Collins, S. M. Tikoo, C. Verhagen, G. L. Christeson, P. Claeys, M. J. L. Coolen, S. Goderis, K. Goto, R. A. F. Grieve, N. M. Call, G. R. Osinski, A. S. P. Rae, U. Riller, J. Smit, V. Vajda, A. Wittmann; Expedition 364 Scientists, The first day of the Cenozoic. *Proc. Natl. Acad. Sci. U.S.A.* **116**, 19342–19351 (2019).
4. S. D'Hondt, Consequences of the Cretaceous/Paleogene mass extinction for marine ecosystems. *Annu. Rev. Ecol. Evol. Syst.* **36**, 295–317 (2005).
5. K. Kaiho, N. Oshima, K. Adachi, Y. Adachi, T. Mizukami, M. Fujibayashi, R. Saito, Global climate change driven by soot at the K-Pg boundary as the cause of the mass extinction. *Sci. Rep.* **6**, 28427 (2016).
6. C. G. Bardeen, R. R. Garcia, O. B. Toon, A. J. Conley, On transient climate change at the Cretaceous–Paleogene boundary due to atmospheric soot injections. *Proc. Natl. Acad. Sci. U.S.A.* **114**, E7415–E7424 (2017).
7. M. J. Henehan, A. Ridgwell, E. Thomas, S. Zhang, L. Alegret, D. N. Schmidt, J. W. B. Rae, J. D. Witts, N. H. Landman, S. E. Greene, B. T. Huber, J. R. Super, N. J. Planavsky, P. M. Hull, Rapid ocean acidification and protracted Earth system recovery followed the end-Cretaceous Chicxulub impact. *Proc. Natl. Acad. Sci. U.S.A.* **116**, 22500–22504 (2019).
8. P. R. Bown, J. A. Lees, J. R. Young, Calcareous nannoplankton evolution and diversity through time, in *Coccolithophores–From Molecular Processes to Global Impacts*, H. Thierstein, J. R. Young, Eds. (Springer, 2004), pp. 481–508.
9. S. A. Alvarez, S. J. Gibbs, P. R. Bown, H. Kim, R. M. Sheward, A. Ridgwell, Diversity decoupled from ecosystem function and resilience during mass extinction recovery. *Nature* **574**, 242–245 (2019).
10. H. S. Birch, H. K. Coxall, P. N. Pearson, D. Kroon, D. N. Schmidt, Partial collapse of the marine carbon pump after the Cretaceous-Paleogene boundary. *Geology* **44**, 287–290 (2016).
11. M. J. Henehan, P. M. Hull, D. E. Penman, J. W. B. Rae, D. N. Schmidt, Biogeochemical significance of pelagic ecosystem function: An end-Cretaceous case study. *Philos. Trans. R. Soc. B* **371**, 20150510 (2016).

12. L. Alegret, E. Thomas, Deep-Sea environments across the Cretaceous/Paleogene boundary in the eastern South Atlantic Ocean (ODP Leg 208, Walvis Ridge). *Mar. Micropaleontol.* **64**, 1–17 (2007).
13. J. Sepúlveda, J. E. Wendler, E. Summons, Roger, K.-U. Hinrichs, Rapid resurgence of marine productivity after the Cretaceous-Paleogene mass extinction. *Science* **326**, 129–132 (2009).
14. B. Schaefer, K. Grice, M. J. L. Coolen, R. E. Summons, X. Cui, T. Bauersachs, L. Schwark, M. E. Böttcher, T. J. Bralower, S. L. Lyons, K. H. Freeman, C. S. Cockell, S. P. S. Gulick, J. V. Morgan, M. T. Whalen, C. M. Lowery, V. Vajda, Microbial life in the nascent Chicxulub crater. *Geology* **48**, 328–332 (2020).
15. H. Brinkhuis, H. Leereveld, Dinoflagellate cysts from the Cretaceous/Tertiary boundary sequence of El Kef, northwest Tunisia. *Rev. Palaeobot. Palynol.* **56**, 5–19 (1988).
16. P. A. Sims, D. G. Mann, L. K. Medlin, Evolution of the diatoms: Insights from fossil, biological and molecular data. *Phycologia* **45**, 361–402 (2006).
17. S. Ribeiro, T. Berge, N. Lumdholm, T. J. Andersen, F. Abrantes, M. Ellegaard, Phytoplankton growth after a century of dormancy illuminates past resilience to catastrophic darkness. *Nat. Commun.* **2**, 311 (2011).
18. J. J. Pospichal, Calcareous nannoplankton mass extinction at the Cretaceous/Tertiary boundary: An update, in *The Cretaceous-Tertiary Event and Other Catastrophes in Earth History*, G. Ryder, D. E. Fastovsky, S. Gartner, Eds. (GSA Special Paper 307, Geological Society of America, 1996), pp. 335–360.
19. P. Bown, Selective calcareous nannoplankton survivorship at the Cretaceous-Tertiary boundary. *Geology* **33**, 653–656 (2005).
20. A. Houdan, I. Probert, C. Zatylny, B. Vérnon, C. Billard, Ecology of oceanic coccolithophores. I. Nutritional preferences of the two stages in the life cycle of *Coccolithus braarudii* and *Calcidiscus leptoporus*. *Aquat. Microb. Ecol.* **44**, 291–301 (2006).
21. L. Cros, M. Estrada, Holo-heterococcolithophore life cycles: Ecological implications. *Mar. Ecol. Prog. Ser.* **492**, 57–68 (2013).
22. A. Winter, R. W. Jordan, P. H. Roth, Biogeography of living coccolithophores in ocean waters, in *Coccolithophores*, A. Winter, W. G. Siesser, Eds. (Cambridge Univ. Press, 1994), pp. 161–178.
23. J. Godrijan, J. R. Young, D. Marić Pfannkuchen, R. Precali, M. Pfannkuchen, Coastal zones as important habitats of coccolithophores: A study of species diversity, succession, and life-cycle phases. *Limnol. Oceanogr.* **63**, 1692–1710 (2018).
24. See Materials and Methods and Supplementary Materials.
25. H. L. Jones, B. S. C. Leadbeater, J. C. Green, Mixotrophy in haptophytes, in *The Haptophyte Algae*, J. C. Green, B. S. C. Leadbeater, Eds. (Systematics Association Special, Clarendon Press, 1994), vol. **51**, pp. 247–263.
26. J. Dölger, L. T. Nielsen, T. Kiørboe, A. Andersen, Swimming and feeding of mixotrophic biflagellates. *Sci. Rep.* **7**, 39892 (2017).
27. J. R. Young, P. R. Bown, J. A. Lees, Nannotax3 website (2020); www.mikrotax.org/Nannotax3/.
28. M. Kawachi, I. Inouye, Functional roles of the haptonema and the spine scales in the feeding process of *Chrysochromulina spinifera* (Fournier) Pienaar et Norris (Haptophyta = Prymnesiophyta). *Phycologia* **34**, 193–200 (1995).
29. W. Eikrem, L. K. Medlin, J. Henderiks, S. Rokitta, B. Rost, I. Probert, J. Throndsen, B. Edvardsen, Haptophytes, in *Handbook of the Protists*, J. M. Archibald A. G. B. Simpson, C. H. Slamovits, L. Margulis, Eds. (Springer, 2016), pp. 1–59.
30. R. A. DePalma, J. Smit, D. A. Burnham, K. Kuiper, P. L. Manning, A. Oleinik, P. Larson, F. J. Maurrasse, J. Vellekoop, M. A. Richards, L. Gurche, W. Alvarez, A seismically induced onshore surge deposit at the KPg boundary, North Dakota. *Proc. Natl. Acad. Sci. U.S.A.* **116**, 8190–8199 (2019).
31. L. K. Medlin, A. G. Sáez, J. R. Young, A molecular clock for coccolithophores and implications for selectivity of phytoplankton extinctions across the K/T boundary. *Mar. Micropal.* **67**, 69–86 (2008).
32. F. Unrein, J. M. Gasol, F. Not, I. Forn, R. Massana, Mixotrophic haptophytes are key bacterial grazers in oligotrophic coastal waters. *ISME J.* **8**, 164–176 (2014).
33. J. M. Burkholder, P. M. Glibert, H. M. Skelton, Mixotrophy, a major mode of nutrition for harmful algal species in eutrophic waters. *Harmful Algae* **8**, 77–93 (2008).
34. D. K. Stoecker, P. J. Lavrentyev, Mixotrophic plankton in the polar seas: A pan-arctic review. *Front. Mar. Sci.* **5**, 292 (2018).
35. D. H. Erwin, The end and the beginning: Recoveries from mass extinctions. *Trends Evol. Ecol.* **13**, 344–349 (1998).
36. D. P. G. Bond, S. E. Grasby, On the causes of mass extinctions. *Palaeogeogr. Palaeoclimatol. Palaeoecol.* **478**, 3–29 (2017).
37. C. H. Ellis, W. H. Lohmann, Toweius petalosus new species, a Paleocene calcareous nannofossil from Alabama. *Tulane Stud. Geol. Paleontol.* **10**, 107–110 (1973).
38. H. Mai, New coccolithophorid taxa from Geulhemmerberg airshaft, lower Paleocene, The Netherlands. *Micropaleontology* **47**, 144–154 (2001).
39. H. Mai, T. Hildebrand-Habel, K. von Salis Perch-Nielsen, H. Willems, Paleocene coccospheres from DSDP Leg 39, Site 356, São Paulo Plateau, S Atlantic Ocean. *J. Nannoplankton Res.* **20**, 21–29 (1998).
40. W. Wei, J. J. Pospichal, Danian calcareous nannofossil succession at ODP Site 738 in the southern Indian Ocean. *Proc. ODP Sci. Results* **119**, 495–512 (1991).
41. P. R. Bown, J. R. Young, Techniques, in *Calcareous Nannofossil Biostratigraphy,* P. R. Bown, Ed. (Kluwer Academic Publishers, 1998), pp. 16–28.
42. P. R. Bown, T. Dunkley Jones, J. A. Lees, P. N. Pearson, J. R. Young, R. Randell, H. K. Coxall, J. Mizzi, C. J. Nicholas, A. Karega, J. Singano, B. S. Wade, A Paleogene calcareous microfossil Konservat-Lagerstätte from the Kilwa Group of coastal Tanzania. *Geol. Soc. Am. Bull.* **120**, 3–12 (2008).
43. J. A. Lees, P. R. Bown, J. R. Young, J. B. Riding, Evidence for annual records of phytoplankton productivity in the Kimmeridge Clay Formation coccolith stone bands (Upper Jurassic, Dorset, UK). *Mar. Micropaleontol.* **52**, 29–49 (2004).
44. L. Šupraha, Z. Ljubešić, H. Mihanović, J. Henderiks, Observations on the life cycle and ecology of *Acanthoica quattrospina* Lohmann from a Mediterranean estuary. *J. Nannoplankton Res.* **34**, 49–56 (2014).
45. M. Kawachi, I. Inouye, Observations on the Flagellar Apparatus of a Coccolithophorid, *Cruciplacolithus neohelis* (Prymnesiophyceae). *J. Plant Res.* **107**, 53–62 (1994).
46. H. J. Jeong, Y. Du Yoo, J. Y. Park, J. Y. Song, S. T. Kim, S. H. Lee, K. Y. Kim, W. H. Yih, Feeding by phototrophic red-tide dinoflagellates: Five species newly revealed and six species previously known to be mixotrophic. *Aquat. Microb. Ecol.* **40**, 133–150 (2005).
47. Y. Du Yoo, H. J. Jeong, M. S. Kim, N. S. Kang, J. Y. Song, W. Shin, K. Y. Kim, K. Lee, Feeding by phototrophic red-tide dinoflagellates on the ubiquitous marine diatom *Skeletonema costatum*. *J. Eukaryot. Microbiol.* **56**, 413–420 (2009).
48. S. J. Gibbs, P. R. Bown, B. H. Murphy, A. Sluijs, K. M. Edgar, H. Pälike, C. T. Bolton, J. C. Zachos, Scaled biotic disruption during early Eocene global warming events. *Biogeosciences* **9**, 4679–4688 (2012).
49. K. Perch-Nielsen, Cenozoic calcareous nannofossils, in *Plankton Stratigraphy*, H. M. Bolli, J. B. Saunders, K. Perch-Nielsen, Eds. (Cambridge Univ. Press, 1985), pp. 427–554.
50. P. R. Bown, Paleocene calcareous nannofossils from Tanzania (TDP sites 19, 27 and 38). *J. Nannoplankton Res.* **36**, 1–32 (2016).
51. T. Westerhold, U. Röhl, I. Raffi, E. Fornaciari, S. Monechi, V. Reale, J. Bowles, H. F. Evans, Astronomical calibration of the Paleocene time. *Palaeogeogr. Palaeoclimatol. Palaeoecol.* **257**, 377–403 (2008).
52. J. Dinarès-Turell, T. Westerhold, V. Pujalte, U. Röhl, D. Kroon, Astronomical calibration of the Danian stage (Early Paleocene) revisited: Settling chronologies of sedimentary records across the Atlantic and Pacific Oceans. *Earth Planet. Sci. Lett.* **405**, 119–131 (2014).
53. T. Westerhold, U. Röhl, B. Donner, J. C. Zachos, Global extent of early Eocene hyperthermal events: A new Pacific benthic foraminiferal isotope record from Shatsky Rise (ODP Site 1209). *Paleoceanogr. Paleoclimatol.* **33**, 626–642 (2018).
54. R. D. Norris, P. A. Wilson, P. Blum, Expedition 342 Scientists, in *Proceedings of the Integrated Ocean Drilling Program, Volume 342*, R. D. Norris, P .A. Wilson, P. Blum; Expedition 342 Scientists, Eds. (Integrated Ocean Drilling Program, 2014); http://publications.iodp.org/proceedings/342/342toc.htm.
55. J. A. Burnett, Upper Cretaceous, in *Calcareous Nannofossil Biostratigraphy,* P. R. Bown, Ed. (Kluwer Academic Publishers, 1998), pp. 132–165.
56. G. Bernaola, S. Monechi, Calcareous nannofossil extinction and survivorship across the Cretaceous–Paleogene boundary at Walvis Ridge (ODP Hole 1262C, South Atlantic Ocean). *Palaeogeogr. Palaeoclimatol. Palaeoecol.* **255**, 132–156 (2007).
57. N. Thibault, S. Gardin, The calcareous nannofossil response to the end-Cretaceous warm event in the Tropical Pacific. *Palaeogeogr. Palaeoclimatol. Palaeoecol.* **291**, 239–252 (2010).
58. S. J. Gibbs, A. J. Poulton, P. R. Bown, C. J. Daniels, J. Hopkins, J. R. Young, H. L. Jones, G. J. Thiemann, S. A. O'Dea, C. Newsam, Species-specific growth response of coccolithophores to Palaeocene–Eocene environmental change. *Nat. Geosci.* **6**, 218–222 (2013).
59. S. Våge, M. Castellani, J. Giske, T. F. Thingstad, Successful strategies in size structured mixotrophic food webs. *Aquat. Ecol.* **47**, 329–347 (2013).
60. B. A. Ward, M. J. Follows, Marine mixotrophy increases trophic transfer efficiency, mean organism size, and vertical carbon flux. *Proc. Natl. Acad. Sci. U.S.A.* **113**, 2958–2963 (2016).
61. C. T. Reinhard, N. J. Planavsky, B. A. Ward, G. D. Love, G. Le Hir, A. Ridgwell, The impact of marine nutrient abundance on early eukaryotic ecosystems. *Geobiology* **18**, 139–151 (2020).
62. P. J. Hansen, P. K. Bjørnsen, B. W. Hansen, Zooplankton grazing and growth: Scaling with the 2–2,000-μm body size range. *Limnol. Oceanogr.* **42**, 687–704 (1997).
63. B. W. Hansen, P. K. Bjornsen, P. J. Hansen, The size ratio between planktonic predators and their prey. *Limnol. Oceanogr.* **39**, 395–403 (1994).
64. K. F. Edwards, M. K. Thomas, C. A. Klausmeier, E. Litchman, Allometric scaling and taxonomic variation in nutrient utilization traits and maximum growth rate of phytoplankton. *Limnol. Oceanogr.* **57**, 554–566 (2012).

65. D. K. Stoecker, Acquired phototrophy in aquatic protists. *Aquat. Microb. Ecol.* **57**, 279–310 (2009).
66. J. D. van der Laan, P. Hogeweg, Predator—Prey coevolution: Interactions across different timescales. *Proc. R. Soc. Lond. B.* **259**, 35–42 (1995).
67. B. Sauterey, B. Ward, J. Rault, C. Bowler, D. Claessen, The implications of eco-evolutionary processes for the emergence of marine plankton community biogeography. *Am. Nat.* **190**, 116–130 (2017).
68. K. Hagino, J. R. Young, P. R. Bown, J. Godrijan, D. K. Kulhanek, K. Kogame, T. Horiguchi, Re-discovery of a "living fossil" coccolithophore from the coastal waters of Japan and Croatia. *Mar. Micropal.* **116**, 28–37 (2015).
69. N. A. Kamennaya, G. Kennaway, B. M. Fuchs, M. V. Zubkov, "Pomacytosis"—Semi-extracellular phagocytosis of cyanobacteria by the smallest marine algae. *PLOS Biol.* **16**, e2003502 (2018).
70. K. Hagino, R. Onuma, M. Kawachi, T. Horiguchi, Discovery of an endosymbiotic nitrogen-fixing cyanobacterium UCYN-A in *Braarudosphaera bigelowii* (Prymnesiophyceae). *PLOS ONE* **8**, e81749 (2013).
71. C. Linnert, J. Mutterlose, Boreal Early Turonian calcareous nannofossils from nearshore settings – Implications for paleoecology. *PALAIOS* **30**, 728–742 (2015).
72. H. Andruleit, S. Stäger, U. Rogalla, P. Čepek, Living coccolithophores in the northern Arabian Sea: Ecological tolerances and environmental control. *Mar. Micropal.* **49**, 157–181 (2003).
73. H. Mai, K. S. Perch-Nielsen, H. Willems, T. Romein, Fossil coccospheres from the K/T boundary section from Geulhemmerberg, The Netherlands. *Micropaleontology* **43**, 281–302 (1997).
74. J. Monod, La technique de culture continue, théorie et applications. *Ann. Inst. Pasteur* **79**, 390–410 (1950).
75. C. S. Holling, Some characteristics of simple types of predation and parasitism. *Can. Entomol.* **91**, 385–398 (1959).
76. W. C. Gentleman, A. B. Neuheimer, Functional responses and ecosystem dynamics: How clearance rates explain the influence of satiation, food-limitation and acclimation. *J. Plankton Res.* **30**, 1215–1231 (2008).
77. E. Marañón, P. Cermeño, D. C. López-Sandoval, T. Rodríguez-Ramos, C. Sobrino, M. Huete-Ortega, J. M. Blanco, J. Rodríguez, Unimodal size scaling of phytoplankton growth and the size dependence of nutrient uptake and use. *Ecol. Lett.* **16**, 371–379 (2013).
78. K. W. Wirtz, Non-uniform scaling in phytoplankton growth rate due to intracellular light and CO_2 decline. *J. Plankton Res.* **33**, 1325–1341 (2011).
79. D. E. Burmaster, The continuous culture of phytoplankton: Mathematical equivalence among three steady-state models. *Am. Nat.* **113**, 123–134 (1979).
80. B. A. Ward, E. Marañón, B. Sauterey, J. Rault, D. Claessen, The size dependence of phytoplankton growth rates: A trade-off between nutrient uptake and metabolism. *Am. Nat.* **189**, 170–177 (2017).
81. K. H. Andersen, J. E. Beyer, Asymptotic size determines species abundance in the marine size spectrum. *Am. Nat.* **168**, 54–61 (2006).
82. A. Beckmann, C.-E. Schaum, I. Hense, Phytoplankton adaptation in ecosystem models. *J. Theor. Biol.* **468**, 60–71 (2019).
83. N. Hamilton, Mesozoic magnetostratigraphy of Maud Rise, Antarctica, in *Proceedings of the Ocean Drilling Program, Scientific Results*, P. F. Barker, J. P. Kennett, Eds. (Ocean Drilling Program, 1990), vol. 113, pp. 255–260.
84. F. M. Gradstein, J. G. Ogg, M. D. Schmitz, G. M. Ogg, *The Geologic Time Scale 2012* (Elsevier, 2012).
85. R. D. Norris, D. Kroon, A. Klaus, Expedition 171B Scientists, in *Proceedings of the Ocean Drilling Programs Initial Reports, 171B*, R. D. Norris, D. Kroon, A. Klaus, Expedition 171B Scientists, Eds. (Integrated Ocean Drilling Program, 1998).

Acknowledgments: This research used samples provided by the International Ocean Discovery Program. We would also like to additionally thank T. Bralower, H. Birch, and J. Young for loan of samples and slides. **Funding:** We would like to thank the Royal Society for funding B.A.W. through a URF. H.K. was part supported by a UCL Dean's prize. We would also like to thank the European Union for postdoctoral research funding for S.A.A. (grant ERC-2013-CoG-617303). A.R. was partly supported by an award from the Heising-Simons Foundation and via grant ERC-2013-CoG-617303. **Author contributions:** S.J.G., P.R.B., and A.R. conceived and designed the study. S.A.A., H.K., and S.J.G. performed the majority of data collection. B.A.W., B.S., and A.R. designed the model, with assistance from J.W., and B.A.W. performed all model runs and model evolution. P.R.B., H.K., O.A.A., A.J.P., and A.R. contributed to data collection, analysis, and interpretation. S.J.G., P.R.B., and B.A.W. wrote the manuscript, and A.R., S.A.A., and A.J.P. participated in manuscript writing and editing. **Competing interests:** The authors declare that they have no competing interests. **Data and materials availability:** All data needed to evaluate the conclusions in the paper are present in the Supplementary Materials. The model code has the accession number doi.org/10.5281/zenodo.3701302 and can be downloaded from https://github.com/geebes/MCM/tree/1.0. Additional data related to this paper may be requested from the authors.

Submitted 20 May 2020
Accepted 16 September 2020
Published 30 October 2020
10.1126/sciadv.abc9123

Citation: S. J. Gibbs, P. R. Bown, B. A. Ward, S. A. Alvarez, H. Kim, O. A. Archontikis, B. Sauterey, A. J. Poulton, J. Wilson, A. Ridgwell, Algal plankton turn to hunting to survive and recover from end-Cretaceous impact darkness. *Sci. Adv.* **6**, eabc9123 (2020).